Experimental validation of the vibration correlation technique robustness to predict buckling of unstiffened composite cylindrical shells

Franzoni, Felipe; Odermann, Falk; Lanbans, Edgars; Bisagni, Chiara; Andrés Arbelo, Mariano; Degenhardt, Richard

Important note
To cite this publication, please use the final published version (if applicable).
Please check the document version above.

Experimental validation of the vibration correlation technique robustness to predict buckling of unstiffened composite cylindrical shells

Felipe Franzoni[a,b,*], Falk Odermann[a], Edgars Lanbans[c], Chiara Bisagni[c], Mariano Andrés Arbelo[d], Richard Degenhardt[a,b,e]

[a] DLR, Institute of Composite Structures and Adaptive Systems, Braunschweig, Germany
[b] University of Bremen, Faserinstitut Bremen e.V., Bremen, Germany
[c] TU Delft, Delft University of Technology, Faculty of Aerospace Engineering, Delft, the Netherlands
[d] ITA, Technological Institute of Aeronautics, Department of Aeronautics, São José dos Campos, Brazil
[e] PFH, Private University of Applied Sciences Göttingen, Composite Engineering, Campus Stade, Stade, Germany

ABSTRACT

Considering the design of aerospace structures, an experimental campaign is essential for validating the sizing methodology and margins of safety. Particularly for buckling-critical cylindrical shells, the traditional buckling test could lead the specimen to permanent damage. Therefore, the validation of nondestructive experimental procedures for estimating the buckling load of imperfection-sensitive structures from the prebuckling stage is receiving more attention from the industry. In this context, this paper proposes an experimental verification of the robustness of a vibration correlation technique developed for imperfection-sensitive structures. The study comprises three nominally identical unstiffened composite laminated cylindrical shells. Each specimen is tested 10 times for buckling at DLR and, the reproducible results — within a small range of deviation between them — corroborate the equivalence of the cylinders. For the robustness assessment of the vibration correlation technique, two different buckling test facilities are considered. Furthermore, the material properties are recalculated through composite composition rules and the influence of enhanced theoretical buckling loads on the VCT predictions is verified. The experimental campaigns corroborate that the vibration correlation technique provides appropriate estimations representing the influence of the different test facilities; moreover, enhanced theoretical buckling loads can improve the predictions for some of the test cases.

1. Introduction

Composite cylindrical shells are considered for the design of launch vehicles' parts due to their natural optimized strength-to-weight ratio and widen possibilities of design [1]. Considering the load envelope of such applications, the project is mostly driven by buckling, which consists of a big challenge for the validation of the final structure, as the load-bearing capacity of composite laminated cylindrical shells is typically imperfection-sensitive. Therefore, there is inherent interest in the development and validation of nondestructive methods to estimate the buckling load from the prebuckling stage for imperfection-sensitive structures, like the vibration correlation technique (VCT).

The VCT relates an initial model and measured data prior to buckling to estimate the buckling load of the structure, assuring a truly nondestructive experimental procedure. Usually, analytical or finite element (FE) models of the nominal structure are considered as an initial model and the measured data consists of the natural frequency magnitudes associated with vibration tests performed at different axial compression load levels. The VCT approaches are classified into indirect or direct methods [2]. Indirect methods provide an assessment of the actual boundary conditions allowing an update of the initial model, which improves the estimation of the buckling load [3]. On the other hand, direct methods extrapolate an experimentally determined functional relationship between the applied load and the loaded natural frequency to estimate the buckling load, see [4–7] among others.

For simply supported structures, a linear relationship between the total applied load and the square of the loaded natural frequency can be demonstrated for columns, plates [4,8] and, cylindrical shells [8,9]:

$$f^2 + p = 1 \qquad (1)$$

where f is the ratio between the loaded natural frequency $\bar{\omega}_{mn}$ and the unloaded natural frequency ω_{mn}, both associated with the same

---

vibration mode defined by m axial half-waves and n circumferential waves (for cylindrical shells), and p is the ratio between the applied load P and the critical buckling load P_{CR}.

Based on the relationship proposed in Eq. (1), the classic VCT approach consists of plotting the characteristic chart f^2 versus p and adjusting a linear best-fit relationship. The obtained equation is extrapolated to the applied load level where the natural frequency becomes zero, which is directly assumed as the buckling load of the structure [2,8].

The above-described linear relationship is straightforward in the case of a beam structure. Sommerfeld experimentally validated it at the beginning of the 20th century [10]; however, other experiments based on the VCT dated from the 1950s, see for instance [4,11]. For other than simply supported boundary condition, the relationship between the applied load and the squared loaded natural frequency is nonlinear, nevertheless, the classic VCT presents proper estimations for columns considering various boundary conditions, as described in [4,12,13].

Concerning plate structures, the application of the classic technique is limited to imperfection-insensitive structures. For example, in the 1950s, Lurie [4] was not able to validate it considering simply supported flat plates; on the other hand, Chailleux et al. [13] investigated, during the 1970s, simply supported flat plate specimens with small imperfections achieving appropriate estimations and, more recently, Chaves-Vargas et al. [14] applied the classic VCT to flat carbon fiber-reinforced polymer stiffened plates.

Until this point, to define and validate a VCT suitable for the buckling load estimation of imperfection-sensitive structures like plates and shells is an open and important research area [15]. Some authors proposed modified VCT methods addressing imperfection-sensitive structures like curved panels and cylindrical shells [2]. Radhakrishnan [5] proposed a linear extrapolation to the applied load axis based on the last two points of the classic characteristic chart. The author evaluated tubes made of Hostaphan® obtaining exact results for the buckling load estimation by tracking the vibration mode similar to the buckling mode.

Based on the results of 35 VCT experiments conducted at Technion for stiffened cylindrical shells, Segal [16] suggested adjusting an optimal parameter q to raise the natural frequency F (in Hz) so a linear best-fit to the applied load P would lead the VCT estimated buckling load to match exactly the experimental buckling load:

$$F^q = A - BP \tag{2}$$

where A and B are fitting constants.

The author proposed a formulation for q in terms of the main geometric characteristics of the stiffened cylindrical shells. The study succeed in obtaining a substantial reduction in the scatter of the VCT estimated knock-down factors (KDF) when compared to the indirect VCT method based on Eq. (1). Plaut and Virgin [17] also investigated Eq. (2) using an analytical model of a shallow elastic arch with pinned ends, the authors suggested a methodology for determining the upper and lower bounds of the optimal parameter q and, hence, of the estimated buckling load.

Souza et al. [6] proposed a VCT approach for imperfection-sensitive structures through a modified characteristic chart consisting of $(1 - p)^2$ versus $1 - f^4$. In such representation, a linear relationship between the variables is expected, as illustrated in Fig. 1, which considers the published results from [6] for a schematic view of the described VCT.

A best-fit procedure of the experimental results provides the suggested linear equation. The authors proposed evaluating the parametric form $(1 - p)^2$ when the natural frequency is zero ($1 - f^4 = 1$ within the mentioned methodology) for estimating the load level in which the structure is unstable leading to the following relationship:

$$(1 - p)^2 + (1 - \xi^2)(1 - f^4) = 1 \tag{3}$$

where ξ^2 represents the drop of the buckling load due to initial imperfections. Thus, the VCT estimation of the buckling load P_{VCT} is expressed in terms of the positive value of ξ as:
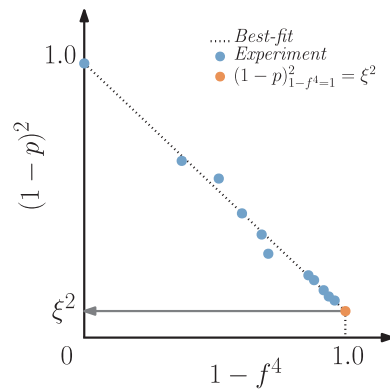
Fig. 1. Schematic view of the VCT proposed in [6].

$$P_{VCT} = P_{CR}(1 - \xi) \tag{4}$$

From Eq. (4), $1 - \xi$ can be compared to the KDF γ of conventional sizing approaches [18].

Souza and Assaid [19] proposed to represent the classic characteristic chart as a cubic parametric curve, in which the parametric equations were obtained through the Hermite form. Both VCT approaches proposed by Souza and his colleagues [6,19] were validated through experimental results of stiffened cylindrical shells tested at Technion [20]. Jansen et al. [21] suggested an extension of the semi-empirical VCT method proposed in [6] by combining it with semi-analytic analysis tools for considering the effects of initial imperfections.

The classic characteristic chart was represented by a second-order best-fit relationship in [15], where the authors evaluated the VCT applied to curved stiffened panels. The predictions accounting for load levels up to 50% of the buckling load of the perfect structure are reasonable; however, the authors suggested load levels near the typical sharp bend of the classic characteristic chart for improving the accuracy.

In 2014, Arbelo et al. [7] proposed an empirical method based on the VCT proposed in [6]. The authors evaluated a second-order best-fit relationship of the modified characteristic chart $(1 - p)^2$ versus $1 - f^2$ leading to the following equation:

$$(1 - p)^2 = A(1 - f^2)^2 + B(1 - f^2) + C \tag{5}$$

where A, B and C are the coefficients determined based on the best-fit procedure of the experimental data. The adjusted second-order equation is minimized and the ξ^2, as defined in [6], is assumed as the correspondent value of $(1 - p)^2$ axis:

$$\min(1 - p)^2 = \xi^2 = -\frac{B^2}{4A} + C \tag{6}$$

The authors suggested estimating the buckling load considering the positive value of ξ as proposed in [6] and here presented in Eq. (4). Fig. 2 shows a schematic view of the described VCT based on the published results from [7].

It is worthy to mention that the above-described VCT is based on the effects of the initial imperfections in the vibration response of the structure and, typically, the first two or three natural frequencies can be evaluated for estimating the buckling load. Furthermore, analytical support for the second-order relationship between the parametric forms $(1 - p)^2$ and $1 - f^2$ and, the insight for a VCT definition based on the minimum value of the parametric form $(1 - p)^2$ are presented in [22].

Until today, the VCT proposed in [7] has been validated based on 7 experimental campaigns for metallic and composite cylindrical shells providing appropriate estimations of the buckling load for the following design details: unstiffened [23–25], with and without cutouts [26], grid-stiffened [27], manufactured considering variable angle tow [28] and, with closely-spaced stringers and internal pressure [29].

To conclude, the buckling performance of composite laminated
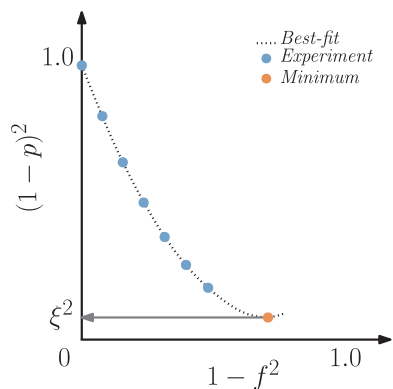
Fig. 2. Schematic view of the VCT proposed in [7].

cylindrical shells is influenced by the test set-up and, by the variations of the geometric and material characteristics, which are inherent of the manufacturing process. In this context, the main contribution of the present article is the validation of the robustness of the VCT via performing the tests campaigns of corroborated equivalent cylinders in two different buckling test facilities. Furthermore, enhanced theoretical buckling loads are proposed and their influence on the VCT estimations is verified.

2. Test structures

This study concerns three nominally equal unstiffened cylindrical shells manufactured at DLR Institute of Composite Structures and Adaptive Systems named ZD27, ZD28, and ZD29. The specimens consist of composite shells fabricated by hand-layup using four plies of the unidirectional carbon fiber prepreg IM7/8552 (Hexcel) and the same mold. Fig. 3 depicts the three cylindrical shells while Table 1 shows the measured geometric characteristics and the correspondent nominal values; additionally, Table 2 presents the mechanical properties of the unidirectional lamina considering 0.125 mm as the nominal ply thickness and a fiber volume fraction of 60.5% [30].

From Table 1, the intrinsic variations of the geometric characteristics of the cylinders are within a tolerable range; moreover, the state-of-the-art techniques for performing such measurements and the preparation of the boundary conditions are described below.

The test specimens were submitted to an ultrasonic scan in order to identify the thickness variation. The thickness measuring was performed through a 10 MHz probe giving a good balance between thickness range and resolution considering the total surface of the cylinders. The average thickness of each specimen is shown in Table 1

while Fig. 4 presents these measurements for each cylindrical shell (in mm).

If one assumes that the thickness variations are associated with the amount of matrix variation, while the amount of fibers remains constant, the material properties of Table 2 can be recalculated through composite composition rules as proposed in [31]. In this study, the material properties are modified taking into account the average thickness presented in Table 1; for the calculation, the elastic modulus of the matrix is 4,670 MPa [32] and the Poisson's ratio is assumed 0.30 as suggested in [31]. Table 3 shows the modified material properties, which are employed to calculate enhanced theoretical buckling loads for each specimen.

Concerning the boundaries of the cylindrical shells, circular steel end plates with rings (20 mm in height) were used to pot the specimen with an epoxy resin. The inner ring has the nominal inner diameter of the cylinder, therefore, no resin area is expected, while the outer ring provides a trapezoidal cross-section for the resin area. Fig. 5 shows a schematic view of the bottom edge of the cylindrical shells (in mm).

Once the cylindrical shells are potted into the metallic rings, a digital image correlation system based on photogrammetry, named ATOS, was used for measuring the outer surface deviations. These measurements allow the calculation of the ideal best-fit cylindrical shell and the correspondent mid-surface best-fit radius of Table 1. Fig. 6 presents the measured outer surface deviation of the specimens (in mm).

3. Linear finite element analysis

Linear buckling analyses based on four FE models are considered to calculate the theoretical buckling loads of the specimens, which are used for the VCT predictions. The study uses the commercial FE solver Abaqus Standard 6.16® for pre- and postprocessing of the numerical models and the linear buckling steps are calculated through the default Lanczos solver. The FE models are defined with clamped boundary conditions at both edges and quadratic quadrilateral shell elements with 8 nodes, 6 degrees of freedom per node and reduced integration; labeled S8R elements.

Firstly, an FE model based on the nominal geometric and material properties, from Tabs. 1 and 2, respectively, is proposed for calculating the nominal theoretical buckling load P_{CR}, which is in practice used for VCT estimations [7,22–29]. Additionally, a numerical model taking into account the measured geometric characteristics from Table 1 and the recalculated material properties from Table 3 is defined for each cylinder. These FE models are employed for calculating enhanced theoretical buckling loads $P_{CR,MOD}$, which reflect the particularities of each specimen. Subsequently, both theoretical buckling loads P_{CR} and $P_{CR,MOD}$ are used for predicting the buckling load of each cylinder.

A convergence analysis taking into account 60, 120, 240, and 480

(a) Cylinder ZD27.

(b) Cylinder ZD28.

(c) Cylinder ZD29.

Fig. 3. Overview of the tested specimens.

Table 1
Geometric characteristics of cylinders ZD27, ZD28, and ZD29.

Description	Nominal	ZD27	ZD28	ZD29
Free length [mm]	560	560	560	560
Mid-surface best-fit radius [mm]	250.00	250.78	250.86	250.87
Average total thickness [mm]	0.50	0.58	0.48	0.52
Lay-up [°]	$[+45 \ -45]_S$	$[+45 \ -45]_S$	$[+45 \ -45]_S$	$[+45 \ -45]_S$

Table 2
Mechanical material properties of the unidirectional lamina IM7/8552 [30].

E_{11} [GPa]	E_{22} [GPa]	ν_{12}	G_{12} [GPa]	G_{13} [GPa]	G_{23} [GPa]	ρ [kg/m^3]
150.00	9.08	0.32	5.29	5.29	5.29	1570

Table 3
Recalculated mechanical material properties based on [31].

Cylinder	E_{11} [GPa]	E_{22} [GPa]	ν_{12}	G_{12} [GPa]	G_{13} [GPa]	G_{23} [GPa]
ZD27	130.82	8.53	0.32	4.67	4.67	4.67
ZD28	155.93	9.26	0.32	5.51	5.51	5.51
ZD29	144.84	8.93	0.32	5.11	5.11	5.11

elements over the circumference with a consistent global size of the elements in other directions (keeping square elements) was performed. The results showed that a converged buckling load (within 1 percent deviation as related to the finest mesh) is achieved for 120 elements over the circumference for the described FE models. The elements in other directions are chosen automatically by the program considering a global size of approximately 13.09, 13.13, 13.14, and 13.14 mm for the FE models defined based on the nominal, ZD27, ZD28, and ZD29 cylinders, respectively. Thus, the FE models have 5,040 S8R shell elements associated with 15,360 nodes. Fig. 7(a) presents an overview of the FE mesh and Fig. 7(b) the described convergence analysis where the deviation is related to the finest mesh.

The numerical results of the above-described theoretical linear buckling loads, P_{CR} and $P_{CR,MOD}$, are summarized in Table 4.

Considering the proposed FE models, the first linear buckling mode is helical and associated with 15 angled axial half-waves and 1 circumferential wave. Furthermore, analyzing Table 4, one may notice that a greater magnitude of the linear buckling load $P_{CR,MOD}$ is obtained for cylinders ZD27 and ZD29 and, a smaller one for cylinder ZD28 when compared to the buckling load of the nominal cylinder P_{CR}.

4. Experimental campaigns

The VCT test campaign consists of a sequence of vibration tests performed at different load levels. In this study, firstly, the three specimens were tested 10 times for buckling at DLR establishing the correspondence between the cylinders. After that, for corroborating the robustness of the VCT method proposed in [7], the VCT test campaigns are performed in two different buckling test facilities. Cylinders ZD28 and ZD29 were tested for VCT at DLR and cylinder ZD27 was tested for VCT at TU Delft. For establishing a basis of comparison between the test facilities, cylinder ZD27 was also tested for buckling at TU Delft. This section describes the procedures for the test campaigns performed in both locations.

4.1. DLR test procedures and results

The DLR experimental campaign consisting of buckling and vibration tests were performed in a dynamic buckling test facility at DLR

Fig. 5. Schematic detailed view of the bottom edge.

Institute of Composite Structures and Adaptive Systems. The test rig consists of a lower base plate with a load releasing structure on the bottom of the test rig and a top drive unit activated by a linear electric actuator. This load introduction unit is guided by linear bearings at three positions so that the only possible translation is the axial direction of the cylinder. Additionally, it acts as a load distributor to ensure an equal force distribution.

Below the load releasing structure, 3 load cells are mounted, which were used for measuring the applied axial load. Moreover, the relative displacement of the load introduction with respect to the load releasing structure is also measured by three displacement sensors that are placed equally distributed around the circumference of the cylinder.

Furthermore, the interfaces between the lower end plate and the load releasing structure as well as the interface between the top end plate and the load introduction were filled with a thin-layer of epoxy concrete. These layers consist of epoxy resin reinforced with a mixture of sand and quartz powder aiming to reduce any additional misalignment. Fig. 8(a) presents cylinder ZD28 positioned in the described test facility and Fig. 8(b) a detailed view of the shaker coupled at cylinder ZD28.

Displacement control was used to load the structures at a 0.8 mm/

(a) Cylinder ZD27.   (b) Cylinder ZD28.   (c) Cylinder ZD29.
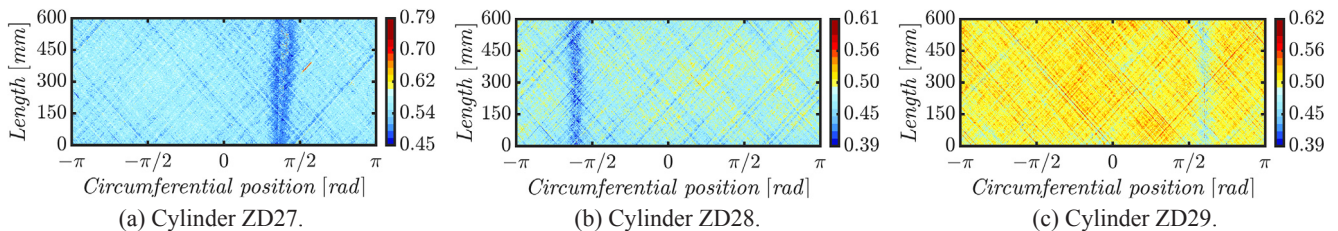
Fig. 4. Measurements of the thickness variation.

(a) Cylinder ZD27.

(b) Cylinder ZD28.
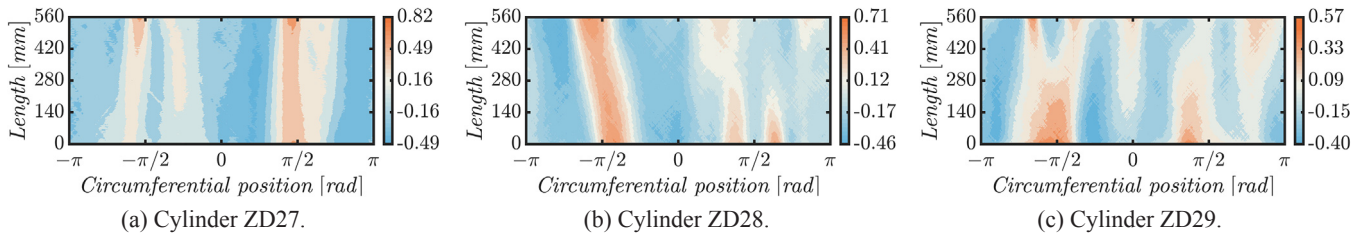
(c) Cylinder ZD29.

Fig. 6. Measurements of the outer surface deviation.

(a) FE mesh overview.

(b) Convergence analysis.
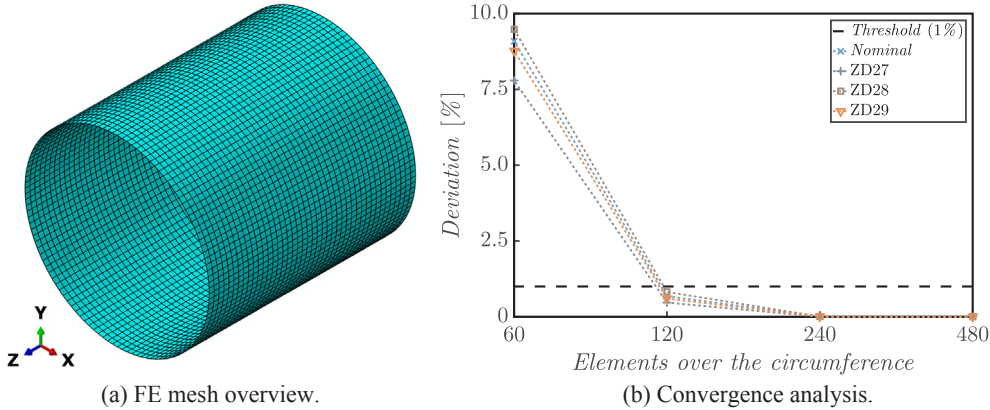
Fig. 7. FE mesh overview and convergence analysis.

Table 4
Numerical results of the linear buckling loads.

Cylinder	P_{CR} [kN]	$P_{CR,MOD}$ [kN]
ZD27	23.43	27.43
ZD28		22.49
ZD29		24.36

min rate. For the VCT tests, the top drive plate is held at the desired load level for performing the vibration test, while for the buckling tests the displacement is applied until buckling takes place.

A mechanical shaker applied the vibration through a rod, seen in Fig. 8(b) and, a laser scanning vibrometer measured the radial velocity

response of the shell surface. The cylindrical shells were exited with a pseudo-random signal. Moreover, two different test configurations were defined for cylinders ZD28 and ZD29, respectively: (1) considers 77 points for measuring the vibration response with a frequency band of 2 kHz and a frequency resolution of 312.5 mHz and, (2) considers 171 points for measuring the vibration response with a frequency band of 1 kHz and a frequency resolution of 156.25 mHz. Additionally, three measurements were taken for averaging the signal for both configurations. Fig. 9 depicts the described grids of measured vibration points for cylinders ZD28 and ZD29.

Ten buckling tests were performed at DLR for each one of the three cylindrical shells. Table 5 presents the results of the 10 buckling tests in terms of the average buckling load P_{EXP} with the correspondent standard deviation. Moreover, two KDF γ are presented for each cylinder,

(a) Cylinder ZD28 positioned in the test facility.

(b) Shaker with rod coupled at cylinder ZD28.

Fig. 8. Overview of the DLR test set-up of cylinder ZD28.

(a) Cylinder ZD28.   (b) Cylinder ZD29.
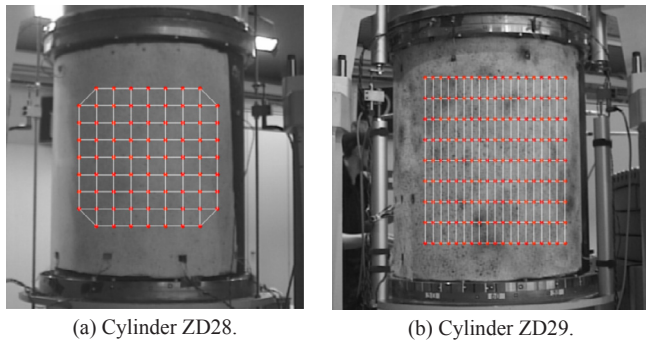
Fig. 9. Grids of the measured vibration points.

Table 5
DLR experimental results of the buckling tests and respective KDF.

Cylinder	P_{EXP} [kN]	γ_{NOM}	γ_{MOD}
ZD27	20.47 ± 0.0065	0.87	0.75
ZD28	21.49 ± 0.0524	0.92	0.96
ZD29	21.86 ± 0.0163	0.93	0.90

one based on the nominal buckling load γ_{NOM} (calculated as P_{EXP}/P_{CR}) and a second based on the enhanced theoretical buckling load γ_{MOD} (calculated as $P_{CR}/P_{CR,MOD}$).

Analyzing Table 5, the sets of 10 buckling tests were reproducible and the results are within an acceptable range of variation corroborating the three specimens as equivalent. Furthermore, the measured geometric characteristics and the modified material properties result in a smaller KDF for ZD27 and ZD29 and a greater one for ZD28.

Concerning the VCT tests performed at DLR, the vibration measurements were performed at 6 load steps for cylinder ZD28 and at 11 load steps for cylinder ZD29. As a result, the study also experimentally verifies the effectiveness of considering a greater number of load steps in the VCT estimations. Fig. 10 shows the first unloaded vibration mode of cylinders ZD28 and ZD29 while Table 6 presents the respective first natural frequency $F_{1,(m,n)}$ variation as related to the applied axial load level P_l.

Evaluating Fig. 10, the first vibration modes of cylinders ZD28 and ZD29 are similar as well as the magnitudes of the first natural frequencies of comparable load steps in Table 6. Given these aspects, one may conclude that the different vibration test configurations of ZD28 and ZD29 are equivalent.

4.2. TU Delft test procedures and results

TU Delft Faculty of Aerospace Engineering performed independent buckling and vibration tests for cylinder ZD27. The compression set-up considers an MTS 3500 servo-hydraulic test machine. The cylinder is placed between the base plate and the compression plate of the machine. Two LVDT (Linear Variable Differential Transformer) sensors are located on both sides of the cylinder to measure the axial shortening. Fig. 11 presents an overview of the described test machine with

(a) Cylinder ZD28 (203.13 Hz).   (b) Cylinder ZD29 (203.75 Hz).

Fig. 10. First unloaded vibration mode of ZD28 and ZD29.

Table 6
DLR experimental results of the vibration tests of cylinders ZD28 and ZD29.

ZD28		ZD29	
P_l [kN]	$F_{1,(1,9)}$ [Hz]	P_l [kN]	$F_{1,(1,9)}$ [Hz]
0.38	203.13	0.53	203.75
5.38	194.38	2.96	200.00
10.38	182.81	5.39	195.00
15.38	170.63	7.95	190.00
17.88	165.00	10.41	184.22
20.38	155.31	12.37	180.47
		14.39	175.16
		16.35	170.31
		18.47	164.53
		20.47	157.34
		20.93	153.91

Fig. 11. Cylinder ZD27 positioned in the TU Delft test machine.

cylinder ZD27 positioned for the tests.

The cylinder was loaded in axial compression with displacement driven test mode up to buckling. The displacement speed was set to 0.2 mm/min with the preload value of 1 kN. For the vibration tests, the natural frequencies of the cylinder were measured at various load levels through a test set-up consisting of a laser scanning vibrometer and a loudspeaker. A frequency sweep signal was used for exciting the structure in the range between 100 and 400 Hz with a frequency resolution of 250 mHz. The cylinder was scanned in 146 points considering four measurements for averaging the signal. The described measure grid is presented in Fig. 12.

Cylinder ZD27 failed after the first buckling test, therefore, the experimental buckling load of a single buckling test, the deviation as related to the DLR equivalent test δ_{DLR} and, the correspondent KDF, γ_{NOM} and γ_{MOD}, are presented in Table 7.

From Table 7, the experimental buckling load obtained at TU Delft
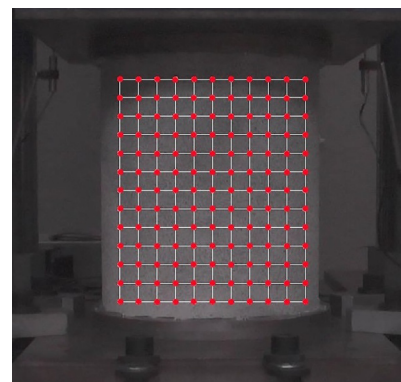
Fig. 12. Grid of the measured vibration points of cylinder ZD27.

Table 7
TU Delft experimental result of the buckling test and respective KDF.

Cylinder	P_{EXP} [kN]	δ_{DLR} [%]	γ_{NOM}	γ_{MOD}
ZD27	15.90	− 22.33	0.68	0.58

(a) 5 kN (176.5 Hz).   (b) 6 kN (175.0 Hz).
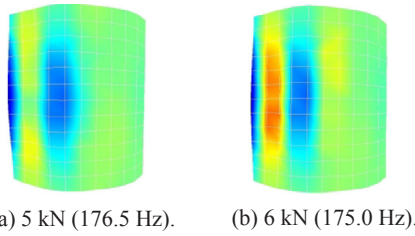
Fig. 13. First vibration mode of ZD27 at 5 and 6 kN.

Table 8
TU Delft experimental results of the vibration tests of cylinder ZD27.

P_i [kN]	$F_{1,(1,9)}$ [Hz]
5.0	176.5
6.0	175.0
7.0	171.5
8.0	168.5
9.0	167.0
10.0	164.0
11.0	161.0
13.0	153.0

(a) Characteristic chart considering $p = P_i/P_{CR}$.

(b) Characteristic chart considering $p = P_i/P_{CR,MOD}$.

Fig. 14. VCT estimations of cylinders ZD27, ZD28, and ZD29.

is considerably smaller when compared to the DLR test result of the same cylindrical shell—22.33% of deviation. This fact can be associated with the differences between the test set-ups, as for instance, load asymmetry (reduced in DLR test arrangement due to the thin-layers of epoxy concrete), boundary conditions, among others. This discrepancy supports the need for the verification of the robustness of the VCT when applied to imperfection-sensitive structures. Additionally, from Table 7, the measured geometric characteristics and the modified material properties result in a smaller magnitude of the KDF for ZD27.

The natural frequencies of the cylinder were measured considering a load step of 1 kN starting from 5 kN, with exception of 12 kN. Lower load levels were not measured due to the not completely fixed boundary conditions at low load magnitudes, noticed previously in similar tests. As there was no adhesive paste added between the cylinder rings and the support plate of the test machine, the cylinder could not be uniformly pressed without applying a certain load level.

Therefore, the present paper also evaluates if the methodology proposed in [7] is applicable when the natural frequency is not available for the unloaded condition. Fig. 13 shows the first vibration mode of cylinder ZD27 at 5 and 6 kN while the variation of first natural frequency $F_{1,(m,n)}$ for the measured load steps P_i are presented in Table 8.

From Fig. 13, it can be noticed that the first vibration modes are slightly different when the results at 5 and 6 kN are compared, this discrepancy can be associated with the not completely fixed set-up. Moreover, comparing the frequency results of the same load level between Tables 6 and 8, it can be seen that the obtained values are much lower when the TU Delft test rig is used, which is a clear indication of more flexible boundary conditions or non-uniform load distribution of the mentioned set-up.

5. Experimental validation of the vibration correlation technique

The method proposed in [7] has been also validated for the second natural frequency in [24]; however, for the specimens herein evaluated,
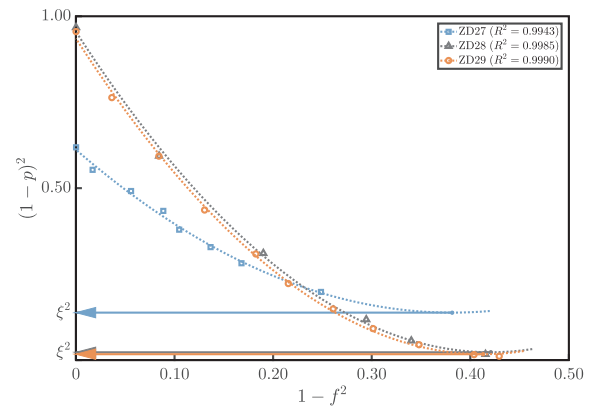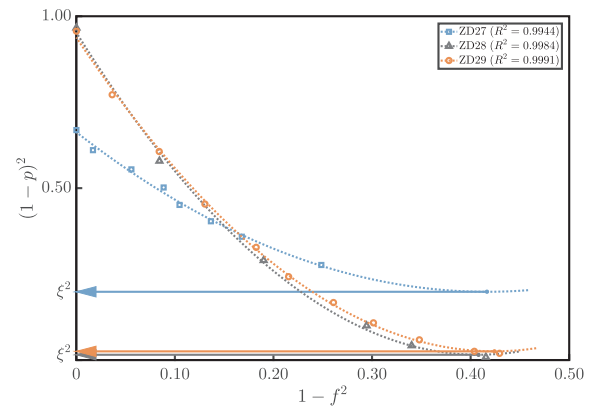
these measurements are not available for all measured load levels. Thus, the following steps are applied for the VCT evaluation:

1. Calculate the critical buckling load of the perfect structure. Two theoretical buckling loads are calculated: (1) the linear buckling load based on the nominal geometric and material properties of the cylinder P_{CR}, as suggested in the literature [7,22–29], and, (2) the linear buckling load of each cylinder based on the measured geometric characteristics and the recalculated material properties $P_{CR,MOD}$. These results are shown in Table 4.
2. Assess the first natural frequency variation during axial loading. This step is performed experimentally in two different buckling test facilities. The results of ZD28 and ZD29 are presented in Table 6 and, the results of ZD27 are shown in Table 8.
3. Generate the charts $(1 − p)^2$ versus $1 − f^2$, where p is the ratio of applied axial load P_i and the considered theoretical buckling load from the linear numerical models (P_{CR} or $P_{CR,MOD}$) and f is the ratio of the first natural frequency at P_i load level $F_{1,(m,n)}$ and the first natural frequency in the unloaded condition. Note that the unloaded condition is not available for the experimental test carried out at TU Delft; therefore, the corresponding natural frequency for the smallest load level (at 5 kN) will be used.
4. Estimate the second-order best-fit relationship between $(1 − p)^2$ and $1 − f^2$, as presented in Eq. (5) and, minimize the quadratic equation for evaluating the square of the drop of the load-carrying capacity ξ^2, as proposed in Eq. (6).
5. Estimate the buckling load of the structure using ξ as proposed by Souza [6] and herein presented in Eq. (4).

Table 9
Summary of the VCT results.

Cylinder	P_{MAX} [%]	P_{EXP} [kN]	$p = P_i/P_{CR}$				$p = P_i/P_{CR,MOD}$			
			ξ^2	P_{VCT} [kN]	γ_{VCT}	δ [%]	ξ^2	P_{VCT} [kN]	γ_{VCT}	δ [%]
ZD27	81.76	15.90	0.1379	14.73	0.63	−7.36	**0.1985**	**15.21**	**0.55**	**−4.35**
ZD28	**94.85**	**21.49**	**0.0226**	**19.91**	**0.85**	**−7.36**	0.0153	19.71	0.88	−8.30
ZD29	95.74	21.86	0.0170	20.37	0.87	−6.81	**0.0253**	**20.49**	**0.84**	**−6.28**

The results considering the load ratio normalized by the critical buckling load based on the nominal geometric and material properties $p = P_i/P_{CR}$ are presented in Fig. 14(a) and, the results for the load ratio normalized by the critical buckling load based on the measured geometric characteristics, and the modified material properties $p = P_i/P_{CR,MOD}$ are shown in Fig. 14(b).

The results of cylinder ZD27 contains a higher scatter within the measured points as compared to ZD28 and ZD29. This fact could be explained by the differences between the test set-ups as well as by the employment of the test machine of TU Delft in the lower range of its load capacity.

Table 9 summarizes the estimated ξ^2, the VCT predicted buckling load P_{VCT}, the respective deviations δ as related to the correspondent experimental buckling load P_{EXP}, the maximum load level considered for the VCT estimation P_{MAX} (in terms of P_{EXP}) and, the correspondent KDF γ_{VCT}.

Analyzing Fig. 14, the experimental results are following the proposed second-order relationship between the parametric variables $(1 - p)^2$ and $1 - f^2$, even in the vicinity of buckling, where the non-linearities are driving the structures' behavior. This can be verified in the experimental campaigns of cylinders ZD28 and ZD29, where the maximum load levels are 94.85 and 95.74%, respectively. Moreover, the adjusted curves are associated with high magnitudes of R^2, which indicates that the proposed equation appropriately fits the experimental data.

From Table 9, the predicted buckling loads are conservative as they are associated with negative deviations. The study provides experimental evidence that the VCT methodology proposed in [7] is more suitable for smaller values of the KDF, as the predictions of ZD27 are in better agreement even considering a relatively smaller maximum load level (81.76% of the corresponded P_{EXP}). Additionally, concerning the use of the nominal theoretical buckling load P_{CR} or the enhanced theoretical buckling load $P_{CR,MOD}$ for calculating the load ratio p, the estimations associated with smaller values of the KDF are in better agreement regardless of the theoretical buckling load considered.

Furthermore, the predictions of ZD27 were not affected by the absence of the unloaded first natural frequency; besides, it is not possible to identify a significant difference between the estimations of ZD28 and ZD29, which indicates that the maximum load level is more effective for reducing the deviations δ than the number of load steps.

6. Final remarks

In this article, the VCT approach proposed in [7] is considered for estimating the buckling load of unstiffened composite laminated cylindrical shells tested in two different test facilities. Three nominal identical specimens were manufactured in DLR Institute of Composite Structures and Adaptive Systems. The three cylinders were tested 10 times each for buckling at DLR, corroborating the equivalence of the specimens. For assessing the robustness of the VCT, ZD28 and ZD29 were tested at DLR and, ZD27 was tested at TU Delft Faculty of Aerospace Engineering. Additionally, a buckling test of ZD27 was performed at TU Delft, which established a basis for comparison between the two buckling test facilities.

Comparing DLR and TU Delft experimental buckling loads of ZD27,

there is 22.33% of deviation as related to the DLR result. This discrepancy can be associated with the differences between the test set-ups and it evidences the need for verifying the robustness of the methodology. The VCT method proposed in [7] predicted within an acceptable range the experimental buckling load of ZD27 (tested at TU Delft) and the buckling loads of ZD28 and ZD29 (both tested at DLR); therefore, the robustness of the methodology of representing the in-situ boundary conditions has been proved throughout this experimental campaign.

The VCT estimations of ZD28 and ZD29 are based on a different number of load steps, 6 and 11, respectively, while the correspondent maximum load levels are similar 94.85 and 95.74%. Moreover, as the test set-up of ZD27 was not fully fixed, the natural frequency was not measured in the unloaded condition for the mentioned specimen; hence, the reference first natural frequency was measured at 5 kN. The results corroborated that the mentioned aspects do not affect the estimations, once the deviations associated with ZD28 and ZD29 are comparable and, the estimations of the buckling load of ZD27 are in good agreement with the respective experimental buckling load.

Furthermore, two theoretical buckling loads (here named P_{CR} and $P_{CR,MOD}$) were considered for the calculation of the load ratio p in the parametric form $(1 - p)^2$. The first buckling load P_{CR} is calculated based on the nominal geometric and material properties, as usually considered in the literature [7,22–29], and, the second $P_{CR,MOD}$ is based on measured geometric characteristics and recalculated material properties (as proposed in [31]). All VCT estimations are conservative (associated with negative deviations) and, in an acceptable range. Moreover, one may notice that the estimations associated with smaller magnitudes of the KDF are in better agreement within the same cylinder regardless of the theoretical buckling load considered for calculating the load ratio p.

Currently, the authors are preparing another experimental campaign to verify the VCT applicability for composite unstiffened cylindrical shells made of thin-ply laminates under internal pressure and considering in-plane imperfections.

Data availability

The raw data required to reproduce these findings cannot be shared at this time due to legal reasons.

References

[1] Labans E, Bisagni C. Buckling and free vibration study of variable and constant-stiffness cylindrical shells. Compos Struct 2019;210:446–57.
[2] Singer J, Arbocz J, Weller T. Buckling experiments: experimental methods in buckling of thin-walled structures. Shells, built-up structures, composites and

additional topics. New York: John Wiley & Sons; 2002.

[3] Singer J, Abramovich H. Vibration correlation techniques for definition of practical boundary conditions in stiffened shells. AIAA J. 1979;17(7):762–9.

[4] Lurie H. Lateral vibrations as related to structural stability. ASME J Appl Mech 1952;19(2):195–204.

[5] Radhakrishnan R. Prediction of buckling strengths of cylindrical shells from their natural frequencies. Earthq Eng Struct Dyn 1973;2:107–15.

[6] Souza MA, Fok WC, Walker AC. Review of experimental techniques for thin-walled structures liable to buckling: neutral and unstable buckling. Exp Tech 1983;7(9):21–5.

[7] Arbelo MA, de Almeida SFM, Donadon MV, Rett SR, Degenhardt R, Castro SGP, et al. Vibration correlation technique for the estimation of real boundary conditions and buckling load of unstiffened plates and cylindrical shells. Thin-Walled Struct 2014;79:119–28.

[8] Virgin LN. Vibration of axially loaded structures. Cambridge: Cambridge University Press; 2007.

[9] A.W. Leissa, Vibration of Shells (NASA SP-288), 1973, US Government Printing Office; Washington.

[10] Sommerfeld A. Eine einfache Vorrichtung zur Veranschaulichung des Knick-un-gsvorganges. Z Des Ver Dtsch Ing 1905;49:1320–3.

[11] Johnson EE, Goldhammer BF. The determination of the critical load of a column or stiffened panel in compression by the vibration method. Proc Soc Exp Stress Anal 1953;11(1):221–32.

[12] Burgreen D. End-fixity effect on vibration and instability. Trans Am Soc Civil Eng 1961;126(1):1058–73.

[13] Chailleux A, Hans Y, Verchery G. Experimental study of the buckling of laminated composite columns and plates. Int J Mech Sci 1975;17:489–98.

[14] Chaves-Vargas M, Dafnis A, Reimerdes H-G, Schröder K-U. Modal parameter identification of a compression-loaded CFRP stiffened plate and correlation with its buckling behaviour. Prog Aerosp Sci 2015;78:39–49.

[15] Abramovich H, Govich D, Grunwald A. Buckling prediction of panels using the vibration correlation technique. Prog Aerosp Sci 2015;78:62–73.

[16] Y. Segal, Prediction of Buckling Load and Loading Conditions of Stiffened Shells from Vibration Tests, M.Sc. Thesis, 1980, Israel Institute of Technology; Haifa, Israel.

[17] Plaut RH, Virgin LN. Use of frequency data to predict buckling. J Eng Mech 1990;116(10):2330–5.

[18] V.I. Weingarten, P. Seide, J.P. Peterson, Buckling of Thin-walled Circular Cylinders (NASA SP-8007), NASA Space Vehicle Design Criteria – Structures (Revised 1968), 1965.

[19] Souza MA, Assaid LMB. A new technique for the prediction of buckling loads from nondestructive vibration tests. Exp Mech 1991;31(2):93–7.

[20] J. Singer, Buckling experiments on shells – a review of recent developments, (Eng. Report TAE No 403), 1980, Technion Israel Institute of Technology.

[21] Jansen EL, Abramovich H, Rolfes R. The direct prediction of buckling loads of shells under axial compression using VCT – towards an upgraded approach. In: Proc. ICAS 2014, 29th Congr. Int. Counc. Aeronaut. Sci. 2014, 1-9; St. Petersburg, Russia.

[22] Franzoni F, Degenhardt R, Albus J, Arbelo MA. Vibration correlation technique for predicting the buckling load of imperfection-sensitive isotropic cylindrical shells: an analytical and numerical verification. Thin-Walled Struct 2019;140:236–47.

[23] Arbelo MA, Kalnins K, Ozolins O, Skukis E, Castro SGP, Degenhardt R. Experimental and numerical estimation of buckling load on unstiffened cylindrical shells using a vibration correlation technique. Thin-Walled Struct 2015;94:273–9.

[24] Kalnins K, Arbelo MA, Ozolins O, Skukis E, Castro SGP, Degenhardt R. Experimental nondestructive test for estimation of buckling load on unstiffened cylindrical shells using vibration correlation technique. Shock Vib 2015;1–8.

[25] Skukis E, Ozolins O, Kalnins K, Arbelo MA. Experimental test for estimation of buckling load on unstiffened cylindrical shells by vibration correlation technique. Procedia Eng 2017;172:1023–30.

[26] Skukis E, Ozolins O, Andersons J, Kalnins K, Arbelo MA. Applicability of the vibration correlation technique for estimation of the buckling load in axial compression of cylindrical isotropic shells with and without circular cutouts. Shock Vib 2017;1–14.

[27] Shahgholian-Ghahfarokhi D, Rahimi G. Buckling load prediction of grid-stiffened composite cylindrical shells using the vibration correlation technique. Compos Sci Technol 2018;167:470–81.

[28] Labans E, Abramovich H, Bisagni C. An experimental vibration-buckling investigation on classical and variable angle tow composite shells under axial compression. J Sound Vib 2019;449:315–29.

[29] Franzoni F, Odermann F, Wilckens D, Skukis E, Kalnins K, Arbelo MA, et al. Assessing the axial buckling load of a pressurized orthotropic cylindrical shell through vibration correlation technique. Thin-Walled Struct 2019;137:353–66.

[30] Bisagni C. Composite cylindrical shells under static and dynamic axial loading: an experimental campaign. Prog Aerosp Sci 2015;78:107–15.

[31] Khakimova R, Wilckens D, Reichardt J, Zimmermann R, Degenhardt R. Buckling of axially compressed CFRP truncated cones: experimental and numerical investigation. Compos Struct 2016;146:232–47.

[32] Hexcel composites, HexPly® 8552 Product Data; 2013.